SCIENTIFIC REPORTS

OPEN

CONFERENCE PROCEEDINGS

APEnergy2014

SUBJECT AREAS:
BATTERIES
CHEMICAL ENGINEERING
SYNTHESIS AND PROCESSING

Received
24 February 2014

Accepted
29 May 2014

Published
29 August 2014

Correspondence and requests for materials should be addressed to Y.C.K. (yckang@konkuk.ac.kr)

Fabrication and electrochemical performance of $0.6Li_2MnO_3$-$0.4Li(Ni_{1/3}Co_{1/3}Mn_{1/3})O_2$ microspheres by two-step spray-drying process

Mun Yeong Son, Jung-Kul Lee & Yun Chan Kang

Department of Chemical Engineering, Konkuk University, 1 Hwayang-dong, Gwangjin-gu, Seoul 143-701, Korea.

$0.6Li_2MnO_3$–$0.4Li(Ni_{1/3}Co_{1/3}Mn_{1/3})O_2$ composite microspheres with dense structures are prepared by a two-step spray-drying process. Precursor powders with hollow and porous structures prepared by the spray-drying process are post-treated at a low temperature of 400°C and then wet-milled to obtain a slurry with high stability. The slurry of the mixture of metal oxides is spray-dried to prepare precursor aggregate powders several microns in size. Post-treatment of these powders at high temperatures (>700°C) produces $0.6Li_2MnO_3$–$0.4Li(Ni_{1/3}Co_{1/3}Mn_{1/3})O_2$ composite microspheres with dense structures and high crystallinity. The mean size and geometric standard deviation of the composite microspheres post-treated at 900°C are 4 μm and 1.38, respectively. Further, the initial charge capacities of the aggregated microspheres post-treated at 700, 800, 900, and 1000°C are 336, 349, 383, and 128 mA h g^{-1}, respectively, and the corresponding discharge capacities are 286, 280, 302, and 77 mA h g^{-1}, respectively. The discharge capacity of the composite microspheres post-treated at an optimum temperature of 900°C after 100 cycles is 242 mA h g^{-1}, and the corresponding capacity retention is 80%.

Micron-sized spherical powders are mainly used as cathode materials for lithium ion batteries (LIBs) because of their high tap density and volumetric energy density[1–5]. Spherical precursor powders several microns in size obtained mainly by co-precipitation methods are reacted with lithium components to form lithium metal oxides of various compositions[4,5]. The spherical shape of the precursor powders is maintained even after the lithiation process. However, co-precipitation methods have a drawback in terms of precise control of the composition of the precursor powders because the precipitation conditions of metal ions are strongly affected by the types of metal components. Lithiation of a co-precipitated product is inevitable because the lithium component cannot be co-precipitated with other metal components. The spray-drying process is also used for the commercial production of cathode materials[6–8]. The mixture of metal oxides or nonsoluble metal salts of each component are milled in a high-energy milling machine to form a slurry for spray drying. Therefore, the uniform mixing of each component comprising the cathode material cannot be achieved in conventional co-precipitation and spray-drying processes.

Spray pyrolysis is advantageous for the preparation of multicomponent oxide powders because microscale reactions occur within droplets that are several microns in size[9–12]. Therefore, spray pyrolysis has been widely employed for the preparation of cathode powders for LIBs. Ultrasonic nebulizers are mainly used for the preparation of spherical cathode powders around one micron in size with a dense structure. However, cathode powders several microns in size cannot be prepared by spray pyrolysis from the droplets generated by an ultrasonic nebulizer. Pneumatic atomizers could be used for the generation of droplets several tens of micrometers in size. However, the morphology of cathode powders obtained by the spray pyrolysis of these droplets cannot be controlled appropriately. Taniguchi et al. prepared micron-sized $LiMn_2O_4$ powders by applying a two-step process[13]. They synthesized $LiMn_2O_4$ powders with a hollow structure by ultrasonic spray pyrolysis at a high temperature of 800°C. The as-prepared $LiMn_2O_4$ powders were then ground using mortar and dispersed into

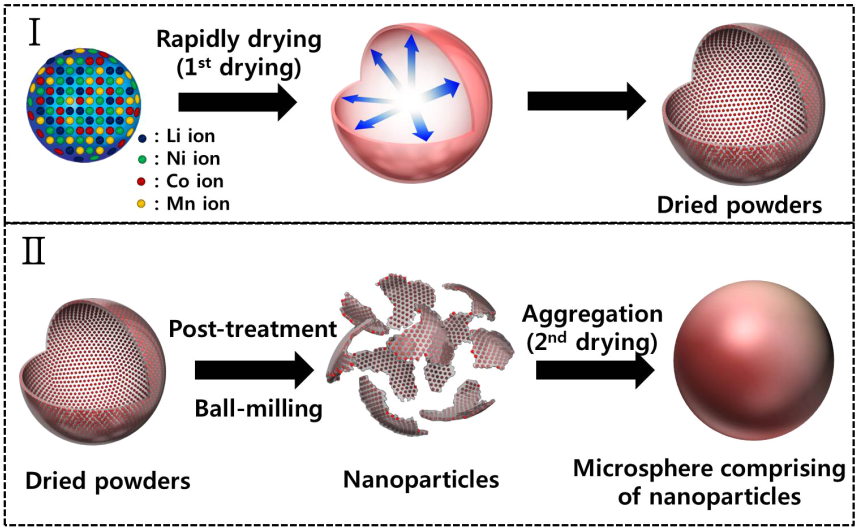

Figure 1 | Formation mechanism of the $0.6Li_2MnO_3$–$0.4Li(Ni_{1/3}Mn_{1/3}Co_{1/3})O_2$ composite microspheres prepared by the two-step spray-drying process.

distilled water. Spherical $LiMn_2O_4$ microparticles were finally prepared from the slurry solution by a spray-drying process.

Li-rich Li–Ni–Mn–Co oxide compounds have mixed-layered crystal structures of the form Li_2MnO_3–$LiMO_2$ (M = Ni, Co, or Mn)[14–16]. Li_2MnO_3 stabilizes the electrode structure and enhances the discharge capacity of the electrode by allowing Li to be extracted concomitant with the release of O (a net loss of Li_2O), typically at voltages in the range 4.6–4.8 V, forming a layered MnO_2 component[17–19]. In particular, Li_2MnO_3–$Li(Ni_{1/3}Co_{1/3}Mn_{1/3})O_2$ materials have been reported to be very promising because of their high capacities[19–22]. The morphology and composition of Li-rich Li–Ni–Mn–Co composite powders need to be precisely controlled for their successful application as cathode materials for LIBs. To improve the electrochemical properties of composite cathode materials, the dispersion of the layered Li_2MnO_3 phase in the layered $LiMO_2$ matrix must be uniform and fine.

In this study, micron-sized $0.6Li_2MnO_3$–$0.4Li(Ni_{1/3}Co_{1/3}Mn_{1/3})O_2$ composite cathode microspheres were prepared by a two-step spray-drying process. The precursor powders for multicomponent cathode powders were prepared from an aqueous spray solution by a spray-drying process. The hollow and thin-walled precursor powders, in which each component was mixed on a molecular level, were prepared by a large-scale spray-drying process. Post-treatment of the precursor powders at a low temperature of 400°C and a subsequent wet-milling process produced a highly stable slurry for the second spray-drying process. The second spray drying of the slurry and the subsequent post-treatment at a high temperature produced cathode microspheres with a dense structure. The physical and electrochemical properties, as well as the formation mechanism of the $0.6Li_2MnO_3$–$0.4Li(Ni_{1/3}Co_{1/3}Mn_{1/3})O_2$ composite microspheres were investigated.

Results

The formation mechanism of the $0.6Li_2MnO_3$–$0.4Li(Ni_{1/3}Mn_{1/3}Co_{1/3})O_2$ composite microspheres prepared by the two-step spray-drying process is shown in Figure 1. Part I of Figure 1 shows the formation mechanism of the dried metal salt powders with hollow and thin-walled structures in the spray-drying process. Droplets containing metal salts came into contact with hot gases in the drying chamber, resulting in the evaporation of the moisture in the droplets. Gas evolution by rapid drying of the droplets resulted in the formation of dried precursor powders with hollow and porous structures. The dried precursor powders were post-treated at a low temperature of 400°C; the post-treated powders were then wet-milled, as shown in Part II of Figure 1. The slurry of the mixture of metal oxides was spray-dried to prepare precursor aggregate powders several microns in size. Post-treatment at high temperatures (>700°C) produced $0.6Li_2MnO_3$–$0.4Li(Ni_{1/3}Mn_{1/3}Co_{1/3})O_2$ microspheres with a dense structure.

The morphology of the precursor powders containing Li, Ni, Co, and Mn components prepared from the aqueous spray solution by the spray-drying process is shown in Figure 2a. The precursor powders had spherical, porous, and hollow structures. Decomposition of metal salts did not occur in the spray-drying process. Therefore, the precursor powders directly prepared by the spray-drying process were a uniform mixture of metal salts of Li, Ni, Co, and Mn components. Further, these precursor powders were completely soluble in water. The metal salts of Mn, Co, Ni, and Li components could not be dried in the spray-drying process because of their high hygroscopicity. Therefore, the precursor powders of the metal salts could not be recovered by a cyclone system without the use of citric acid. However, in this study, citric acid used as a chelating agent enabled the recovery of spray-dried powders by lowering the hygroscopicity of the powders[23]. Figure S1 shows the TG curve of the precursor powders directly obtained by the spray-drying process. The TG curve shows several weight loss steps at temperatures below 700°C. The first weight loss below 200°C was attributed to evaporation of adsorbed water molecules. Several weight loss steps resulting from the decomposition of the metal salts were observed at temperatures between 200 and 450°C. The total weight loss of the precursor powders below 700°C was 65 wt%. The precursor powders obtained by the spray-drying process were post-treated at a low temperature of 400°C in order to change the precursor powders into insoluble metal oxide composite powders. Figure 2b shows the morphology of the post-

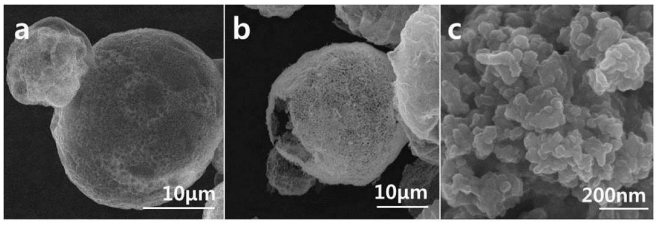

Figure 2 | Morphologies of the Li-Ni-Co-Mn-O precursor powders prepared by spray-drying process.

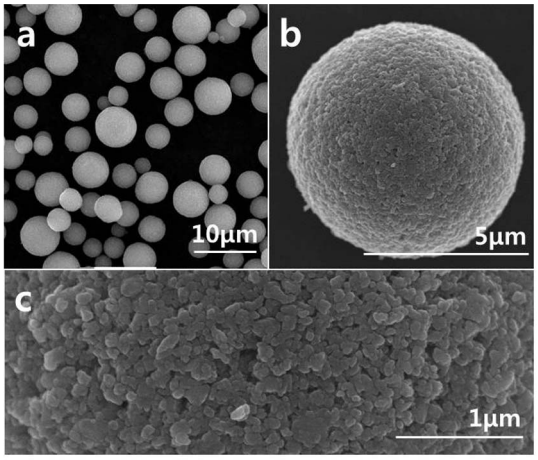

Figure 3 | Morphologies of the aggregated microspheres prepared by second spray-drying process.

treated metal oxide composite powders. The spherical shape of the precursor powders was maintained even after the post-treatment. The decomposition of metal salts produced easily crushable powders. Figure S2 shows the TEM and dot-mapping images of the post-treated metal oxide composite powders. The powders were slightly milled by hand using an agate mortar for the TEM sample. The post-treated powders had aggregated nanostructures of primary nanoparticles several tens of nanometers in size. The dot-mapping images revealed that the Ni, Co, and Mn components were uniformly distributed throughout the powders. Citric acid used as a chelating agent produced precursor powders with uniform composition. The hollow and thin-walled post-treated powders were wet-milled using a planetary mill at 550 rpm for 4 h, resulting in the formation of nanosized powders. The SEM image of the wet-milled powders shown in Figure 2c revealed an ultrafine size and nonaggregation characteristics.

The nanosized primary powders were aggregated into particles several microns in size by using a facile spray-drying method. Figure 3 shows the morphologies of the aggregated microspheres. The highly stable slurry of mixed metal oxides resulted in the formation of spray-dried microspheres with completely spherical shapes, smooth surfaces, dense structures, and nonaggregation characteristics. The high-resolution FE-SEM image shown in Figure 3c shows the aggregated structure of the nanosized precursor powders. The mean size and geometric standard deviation of the aggregated microspheres were 4 μm and 1.38, respectively. The aggregated precursor microspheres obtained by the two-step spray-drying process were post-treated at temperatures between 700 and 1000°C to obtain well-crystallized cathode microspheres. The morphologies of the post-treated $0.6Li_2MnO_3$–$0.4Li(Ni_{1/3}Mn_{1/3}Co_{1/3})O_2$ composite microspheres are shown in Figures 4 and S3. The spherical shape of the microspheres was maintained regardless of the post-treatment temperature. In addition, aggregation between the microspheres did not occur even at a high post-treatment temperature of 1000°C. The distinct crystal growth of the microspheres did not occur at post-treatment temperatures of 700 and 800°C, as shown by the high-resolution SEM images in Figure S3. However, well-grown crystals were observed in the high-resolution SEM images of the microspheres post-treated at 900 and 1000°C. The mean grain sizes of the microspheres post-treated at 900 and 1000°C measured from the SEM images shown in Figure 4b and Figure S3c were 500 and 800 nm, respectively. Figure 4c shows the SEM image of the cross-sections of the aggregated microspheres post-treated at 900°C; the cross-sections were cut by applying a cross-section polisher. This SEM image shows that the aggregated microspheres had filled inner structures. The XRD patterns of the

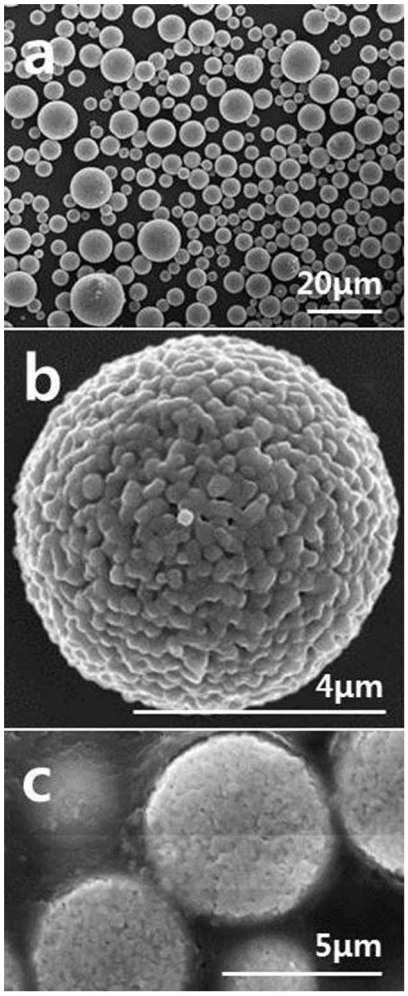

Figure 4 | Morphologies of the aggregated microspheres post-treated at 900°C.

$0.6Li_2MnO_3$–$0.4Li(Ni_{1/3}Mn_{1/3}Co_{1/3})O_2$ composite microspheres post-treated at various temperatures are shown in Figure S4. The microspheres had similar crystal structures irrespective of the post-treatment temperature. The XRD peak near 21°, which can be attributed to the superlattice structure of Li_2MnO_3, was observed at all post-treatment temperatures. Both Li_2MnO_3 and $Li(Ni_{1/3}Co_{1/3}Mn_{1/3})O_2$ had a layered crystal structure; thus, the prepared composite microspheres had mixed-layered crystal structures irrespective of post-treatment temperature. The high $I_{(003)}/I_{(104)}$ peak intensity ratios (>1.3) and the clear splits of the (018)/(110) peaks in the XRD patterns indicate a low amount of cation mixing in the $0.6Li_2MnO_3$–$0.4Li(Ni_{1/3}Mn_{1/3}Co_{1/3})O_2$ composite microspheres irrespective of the post-treatment temperature[23–26]. The mean crystallite sizes of the composite microspheres, measured using Scherrer's equation and the peak widths of the XRD patterns, were 92, 105, 192, and 110 nm at post-treatment temperatures of 700, 800, 900, and 1000°C, respectively. Partial destruction of the structure reduced the mean crystallite size of the composite microspheres post-treated at a high temperature of 1000°C. The N_2 adsorption–desorption isotherms and Barrett–Joyner–Halenda (BJH) pore-size distributions of the layered–layered composite microspheres post-treated at various temperatures are shown in Figure S5. The composite microspheres post-treated at 700°C had well-developed meso- and macropores. However, the composite microspheres post-treated at 900 and 1000°C had dense structures without pores less than 80 nm in size. The Brunauer–Emmett–Teller (BET) surface areas

of the aggregated layered–layered composite microspheres post-treated at 700, 800, 900, and 1000°C were 9.1, 7.4, 3.0, and 1.0 m^2 g^{-1}, respectively, and their pore volumes were 0.11, 0.06, 0.02, and 0.008 cm^3 g^{-1}, respectively. The increase in the post-treatment temperatures decreased the BET surface areas and pore volumes of the microspheres by a densification process. The apparent densities of the aggregated layered–layered composite microspheres post-treated at 700, 800, 900, and 1000°C as measured by mercury porosimetry were 4.2, 3.9, 3.8, and 4.8 g mL^{-1}, respectively. The compositions of the composite microspheres determined by ICP-OES analysis are shown in Table 1. The composite microspheres post-treated at 700, 800, and 900°C had similar compositions. However, the composite microspheres post-treated at 1000°C were slightly lithium-deficient. The compositions of the composite microspheres post-treated at 900 and 1000°C were $Li_{1.21}Ni_{0.10}Co_{0.10}Mn_{0.58}O_2$ and $Li_{1.19}Ni_{0.10}Co_{0.10}Mn_{0.60}O_2$, respectively.

The electrochemical properties of the $0.6Li_2MnO_3$–$0.4Li(Ni_{1/3}Mn_{1/3}Co_{1/3})O_2$ composite microspheres are shown in Figure 5. A cell test was carried out in the voltage range 2.0–4.8 V at a constant current density of 100 mA g^{-1}. Figure 5a shows the initial cycle profile of the layered–layered composite microspheres post-treated at various temperatures. Irrespective of the post-treatment temperature of the composite microspheres, there were two distinct electrochemical reactions as shown by the initial charge curves. It is well known that the smoothly sloping voltage profile below 4.5 V is the result of Li removal from the $Li(Ni_{1/3}Co_{1/3}Mn_{1/3})O_2$ component. The plateau appearing above 4.5 V is attributed to the removal of Li_2O from the Li_2MnO_3 component[14,27,28]. The initial charge capacities of the aggregated microspheres post-treated at 700, 800, 900, and 1000°C were 336, 349, 383, and 128 mA h g^{-1}, respectively, and the corresponding discharge capacities were 286, 280, 302, and 77 mA h g^{-1}, respectively. The initial Coulombic efficiencies of the aggregated microspheres post-treated at 700, 800, 900, and 1000°C were 85, 80, 79, and 60%, respectively. Figure 5b shows the cycling performances of the composite microspheres at a current density of 100 mA g^{-1}. The discharge capacities of the composite microspheres post-treated at 700°C suddenly decreased from 286 to 146 mA h g^{-1} after 100 cycles, and the corresponding capacity retention was 51%. The discharge capacity of the powders post-treated at 1000°C after 100 cycles was low as 52 mA h g^{-1}. However, the composite microspheres post-treated at appropriate temperatures of 800 and 900°C maintained their high discharge capacities. The discharge capacities of the composite microspheres post-treated at high temperatures of 800 and 900°C were 225 and 242 mA h g^{-1}, respectively, and their capacity retentions were each 80%.

The initial differential capacities versus voltage (*dQ/dV*) curves of the layered–layered composite powders post-treated at various temperatures are shown in Figure 6. The initial *dQ/dV* curves of the composite powders showed two distinct oxidation peaks at approximately 4.1 and 4.6 V. The peak at approximately 4.1 V is due to the oxidation of Ni^{2+} to Ni^{4+}. Further, the peak at approximately 4.6 V is due to the irreversible reaction involving the removal of Li and O as Li_2O from Li_2MnO_3[27,29,30]. In the case of the powders post-treated at 1000°C, the oxidation peak resulting from the removal of Li_2O from Li_2MnO_3 shifted toward a higher voltage. The removal of Li_2O from the large-size or large-grain-size Li_2MnO_3 component occurred at high voltages[14,27,31]. Therefore, the peak shifted toward high voltage because the grain sizes of the composite microspheres post-treated at 1000°C were too large. In addition, the large grain size decreased the oxidation peak intensity at approximately 4.6 V. A slight irreversible reaction involving the removal of Li and O as Li_2O from Li_2MnO_3 occurred for the composite microspheres post-treated at 1000°C. Therefore, the composite microspheres post-treated at 1000°C had low initial charge and discharge capacities, as shown in Figure 5. A high amount of the Li_2MnO_3 phase could be formed at high post-treatment temperatures. However, the partial oxidation of the Li_2MnO_3 phase of the composite microspheres with large grain sizes post-treated at a high temperature of 900°C decreased the oxidation peak intensity at approximately 4.6 V in the initial charge process. Therefore, the oxidation peak intensities at around 4.6 V of the composite microspheres post-treated at 700, 800, and 900°C were similar in Figure 6. Because Mn has been shown to exist as Mn^{4+} ions in $Li(Ni_{1/3}Co_{1/3}Mn_{1/3})O_2$, the Mn component did not take part in the redox processes. The MnO_2 formed from Li_2MnO_3 by the elimination of Li_2O in the initial charge process was activated to form $LiMnO_2$ in the subsequent discharge process[14,27,32]. Small reduction peaks ascribed to the reduction of Mn^{4+} to Mn^{3+} were observed below 3.5 V in the initial *dQ/dV* curves shown in the inset of Figure 6[25,27].

Figure 7 shows the subsequent differential capacities versus voltage (*dQ/dV*) curves of the composite microspheres post-treated at

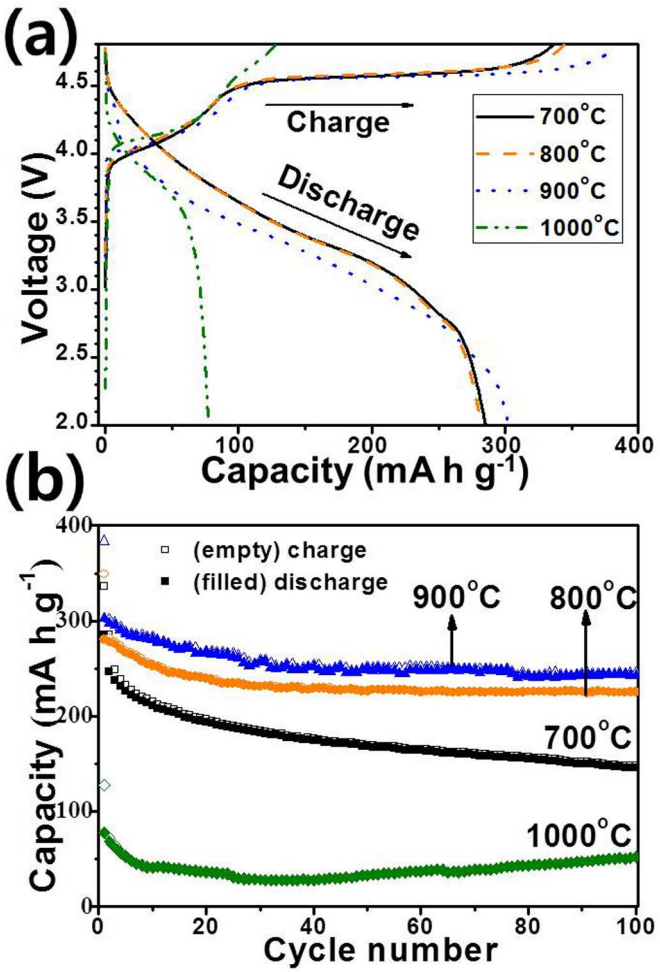

Figure 5 | (a) Initial cycle profiles and (b) cycle performances of the $0.6Li_2MnO_3$-$0.4Li(Ni_{1/3}Co_{1/3}Mn_{1/3})O_2$ microspheres post-treated at various temperatures.

Table 1 | Compositions of the composite microspheres determined by ICP-OES analysis

Temperature	Compositions
700°C	$Li_{1.21}Ni_{0.10}Co_{0.10}Mn_{0.58}O_2$
800°C	$Li_{1.21}Ni_{0.10}Co_{0.10}Mn_{0.58}O_2$
900°C	$Li_{1.21}Ni_{0.10}Co_{0.10}Mn_{0.58}O_2$
1000°C	$Li_{1.19}Ni_{0.10}Co_{0.10}Mn_{0.60}O_2$

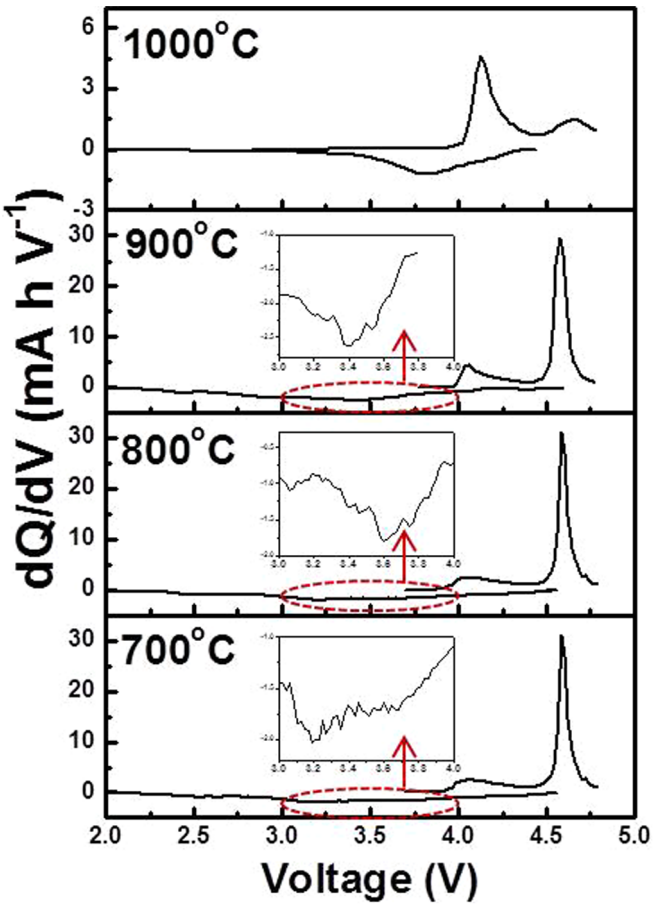

Figure 6 | Initial differential capacities vs. voltage (*dQ/dV*) curves of the $0.6Li_2MnO_3$-$0.4Li(Ni_{1/3}Co_{1/3}Mn_{1/3})O_2$ microspheres post-treated at various temperatures.

various temperatures. The reduction peaks below 3.0 V increased and moved toward low voltages because MnO_2 formed from Li_2MnO_3 by eliminating Li_2O was gradually transformed into spinel $LiMn_2O_4$ through a layered $LiMnO_2$ intermediate as the cycle progressed, as shown in Figures 7a and 7b. The peak below 3.0 V is characteristic of spinel $LiMn_2O_4$[14,22,27]. However, the microspheres post-treated at 900°C maintained their peak intensities at 3.1 V with a slight peak shift and phase transformation during the first 50 cycles. Thus, the microspheres post-treated at 900°C showed stable and good cycling performance. The SEM images and XRD patterns of the powders post-treated at various temperatures after the first cycling are shown in Figures S6 and S7. The powders maintained their spherical morphologies even after cycling regardless of the post-treatment temperatures. The XRD patterns of the powders also showed similar crystal structures even after cycling regardless of the post-treatment temperatures. However, the XRD pattern of the powders post-treated at 1000°C showed a peak near 21°, which can be attributed to the superlattice structure of Li_2MnO_3, even after cycling. The Li_2MnO_3 phase formed at a high post-treatment temperature existed even after cycling. Most of the decrease in the intensity of the superlattice peak (020) during the first charging process was attributed to the irreversible loss of the Li/Mn ordering in Li_2MnO_3 component in the first charging process[33]. The structural stability and high content of the Li_2MnO_3 phase of the powders post-treated at 900°C improved their electrochemical properties.

Discussion

The $0.6Li_2MnO_3$–$0.4Li(Ni_{1/3}Mn_{1/3}Co_{1/3})O_2$ composite microspheres with a large surface area and fine crystallite size post-treated at a low temperature of 700°C had high initial charge/discharge capacities and poor cycling performance. Generally, an increase in the surface area leads to an increase in undesirable side reactions between the electrode and electrolyte and hence to increased capacity fading with cycling. In addition, fast transformation of the Li_2MnO_3 phase into an unstable spinel $LiMn_2O_4$ phase at high operating voltages during the first several cycles resulted in poor cycling performance of the composite microspheres post-treated at a low temperature of 700°C. The $0.6Li_2MnO_3$–$0.4Li(Ni_{1/3}Mn_{1/3}Co_{1/3})O_2$ composite microspheres with a low surface area and optimum grain size post-treated at 900°C had high initial charge/discharge capacities and good cycling performance. However, the large grain size of the composite microspheres post-treated at a high temperature of 1000°C resulted in low charge/discharge capacities during cycling.

In this study, hollow and thin-walled precursor powders, in which each component was mixed on a molecular level, were prepared by a large-scale spray-drying process in order to synthesize multicomponent cathode powders. The post-treatment of the precursor powders at a low temperature of 400°C and the subsequent wet-milling process produced a slurry with high stability for the second spray-drying step. The second spray drying of the slurry and the subsequent post-treatment at high temperatures produced $0.6Li_2MnO_3$–$0.4Li(Ni_{1/3}Mn_{1/3}Co_{1/3})O_2$ composite microspheres with a dense structure. The post-treatment temperature affected the morphology, grain size, and electrochemical properties of the composite microspheres. The optimum post-treatment temperature needed to obtain $0.6Li_2MnO_3$–$0.4Li(Ni_{1/3}Mn_{1/3}Co_{1/3})O_2$ composite microspheres with good electrochemical properties was 900°C. The evaluated composition of the composite microspheres was $Li_{1.21}Ni_{0.10}Co_{0.10}Mn_{0.58}O_2$. The process introduced in this study could be widely applied for the large-scale production of multicomponent cathode powders with spherical shapes, dense structures, and superior electrochemical properties.

Methods

Material fabrication. A commercial spray-drying process (Figure S8) was applied to prepare the precursor powders with a hollow structure. A spray solution containing a high concentration of lithium, nickel, cobalt, and manganese components was pumped into an atomizing device, where it was transformed into a spray of small droplets. These droplets were then brought into contact with a stream of hot air, which resulted in rapid evaporation of the moisture while the droplets were still suspended in the drying air. The dry powder was separated from the humid air by centrifugal forces in a cyclone system. The centrifugal separation was caused by the marked increase in air speed when the mixture of particles and air entered the cyclone system. The temperatures at the inlet and outlet of the spray dryer were 350°C and 150°C, respectively. A two-fluid nozzle was used as an atomizer, and the atomization pressure was 0.3 bar. The spray solution was prepared by dissolving $LiNO_3$ (Junsei, 98%), $Ni(NO_3)_2{\cdot}6H_2O$ (Junsei, 98%), $Mn(NO_3)_2{\cdot}6H_2O$ (Junsei, 97%), and $Co(NO_3)_2{\cdot}6H_2O$ (Junsei, 98%) in distilled water. Citric acid was used as both a chelating agent and a drying additive. The total concentration of metal components in the spray solution was fixed at 0.5 M. The concentration of citric acid was fixed at 0.3 M. The precursor powders obtained by the first spray-drying process were post-treated at a temperature of 400°C for 3 h in air atmosphere. The post-treated powders were milled using a high-speed planetary ball mill for 4 h in deionized water to form a slurry that was spray-dried at 200°C to produce microspheres. In the spry-drying setup, the feeding slurry was pumped to the atomizing device and then sprayed into aerosol droplets. With the hot air flowing, the moisture evaporated in a very short time and spherical powders were produced. Finally, the spray-dried products were annealed at temperatures between 700 and 1000°C for 3 h.

Characterization. The crystal structures of the $0.6Li_2MnO_3$–$0.4Li(Ni_{1/3}Co_{1/3}Mn_{1/3})O_2$ microspheres were investigated using X-ray diffractometry (XRD, DMAX-33, Rigaku) at the Korea Basic Science Institute (Daegu). The morphological characteristics of the samples were investigated using a scanning electron microscope (SEM, JSM-6060, JEOL), field emission SEM (FE-SEM, Hitachi S-4800), and high-resolution transmission electron microscopy (TEM, JEOL JEM-2010). The thermal behavior of the precursor powder obtained by the first spray-drying process was studied by thermal gravimetric analysis (TGA, SDTA851). The samples were heated at a rate of 10°C min^{-1} in the temperature range of 30–700°C. The elemental compositions of the $0.6Li_2MnO_3$–$0.4Li(Ni_{1/3}Co_{1/3}Mn_{1/3})O_2$ microspheres were investigated using an inductively coupled plasma–optical emission spectrometer (ICP-OES, ICAP 6000, Thermo Elemental). The Brunauer–Emmett–Teller (BET) surface areas of the powders were measured using N_2 gas as an

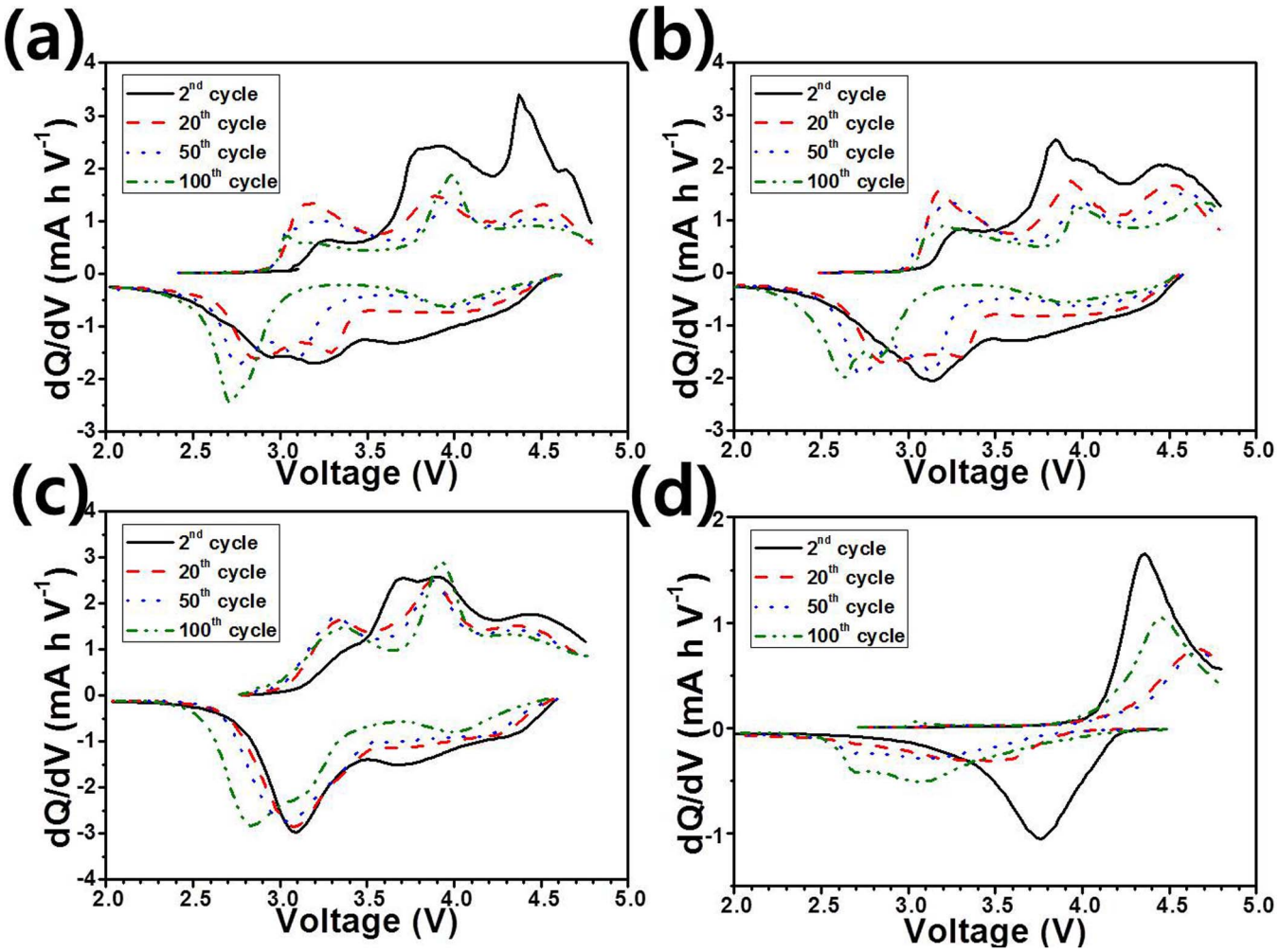

Figure 7 | Subsequent differential capacities vs. voltage (*dQ/dV*) of the $0.6Li_2MnO_3$-$0.4Li(Ni_{1/3}Co_{1/3}Mn_{1/3})O_2$ microspheres post-treated at various temperatures.

adsorbate. The porosities of the powders were measured by mercury porosimeter (Auto Pore IV 9500).

Electrochemical measurements. The capacities and cycling properties of the $0.6Li_2MnO_3$–$0.4Li(Ni_{1/3}Co_{1/3}Mn_{1/3})O_2$ microspheres as a function of the post-treatment temperatures were measured by 2032-type coin cells. The cathode electrode was made of 80 wt% of the $0.6Li_2MnO_3$–$0.4Li(Ni_{1/3}Mn_{1/3}Co_{1/3})O_2$ microspheres, 10 wt% of teflonized acetylene black as a conductive material, and 10 wt% of binder with a few drops of distilled water. All the cathode electrodes were dried at 120°C for 24 h under vacuum. Lithium metal and a polypropylene film were used as the counter electrode and separator, respectively. $LiPF_6$ (1 M) in a mixture of ethylene carbonate (EC) and dimethyl carbonate (DMC) in a 1 : 1 volume was used as the electrolyte. The entire cell was assembled in a glove box under an argon atmosphere. The charge/discharge characteristics of the samples were measured by cycling in the potential range of 2.0–4.8 V at a high current density of 100 mA g^{-1}.

1. Huang, B., Zheng, X., Jia, D. & Lu, M. Design and synthesis of high-rate micron-sized spherical $LiFePO_4$/C composites containing clusters of nano/microsephres. *Electrochim. Acta* **55**, 1227–1231 (2010).
2. MacNell, D. D. *et al.* Melt casting $LiFePO_4$. *J. Electrochem. Soc.* **157**, A463–A468 (2010).
3. Oh, S. W. *et al.* Polyvinylpyrrolidone-assisted synthesis of microscale C-$LiFePO_4$ with high tap density as positive electrode materials for lithium batteries. *Electrochim. Acta* **55**, 1193–1199 (2010).
4. Sun, Y. K. *et al.* High-energy cathode material for long-life and safe lithium batteries. *Nat. Mat.* **8**, 320–324 (2009).
5. Sun, Y. K., Oh, S. M., Park, H. K. & Scrosati, B. Micrometer-sized, nanoporous, high-volumetric-capacity $LiMn_{0.85}Fe_{0.15}PO_4$ cathode material for rechargeable lithium-ion batteries. *Adv. Mater.* **23**, 5050–5054 (2011).
6. Zou, B., Wang, Y. & Zhou, S. Spray drying-assisted synthesis of $LiFePO_4$/C composite microspheres with high performance for lithium-ion batteries. *Mater. Lett.* **92**, 300–303 (2013).
7. Yu, F., Zhang, J., Yang, Y. & Song, G. Porous micro-spherical aggregates of $LiFePO_4$/C nanocomposites: A novel and simple template-free concept and synthesis via sol-gel-spray drying method. *J. Power Sources* **195**, 6873–6878 (2010).
8. Cho, M. Y., Park, S. M., Kim, K. B., Lee, J. W. & Roh, K. C. The synthesis and electrochemical performance of microspherical porous $LiFePO_4$/C with high tap density. *J. Electrochem. Sci. Technol.* **3**, 135–142 (2012).
9. Yang, K. M., Hong, Y. J. & Kang, Y. C. Electrochemical properties of yolk-shell-structured CuO-Fe_2O_3 powders with various Cu/Fe molar ratios prepared by one-pot spray pyrolysis. *ChemSusChem* **6**, 2299–2303 (2013).
10. Hong, Y. J., Son, M. Y., Park, B. K. & Kang, Y. C. One-pot synthesis of yolk-shell materials with single, binary, ternary, quaternary, and quinary systems. *Small* **9**, 2224–2227 (2013).
11. Yang, K. M., Ko, Y. N., Yun, J. Y. & Kang, Y. C. Preparation of $Li_4Ti_5O_{12}$ yolk-shell powders by spray pyrolysis and their electrochemical properties. *Chem. Asian J.* **9**, 443–446 (2014).
12. Hong, Y. J., Yoon, J. W., Lee, J. H. & Kang, Y. C. One-pot synthesis of Pd-loaded SnO_2 yolk-shell nanostructures for ultraselective methyl benzene sensors. *Chem. Eur. J.* **20**, 1–6 (2014).
13. Taniguchi, I., Fukuda, N. & Konarova, M. Synthesis of spherical $LiMn_2O_4$ microparticles by a combination of spray pyrolysis and drying method. *Powder Technol.* **181**, 228–236 (2008).
14. Son, M. Y., Kim, J. H. & Kang, Y. C. Electrochemical properties of $0.6Li_2MnO_3$-$0.4Li(Ni_{1/3}Co_{1/3}Mn_{1/3})O_2$ composite cathode powders with spherical shape and fine size. *Int. J. Electrochem. Sci.* **8**, 2417–2429 (2013).
15. Gan, C., Zhan, H., Hu, X. & Zhou, Y. Origin of the irreversible plateau (4.5 V) of $Li[Li_{0.182}Ni_{0.182}Co_{0.091}Mn_{0.545}]O_2$ layered material. *Electrochem. Commun.* **7**, 1318–1322 (2005).

16. Liu, J. L., Wang, J. & Xiz, Y. Y. A new rechargeable lithium-ion battery with a $xLi_2MnO_3 \cdot (1-x)LiMn_{0.4}Ni_{0.4}Co_{0.2}O_2$ cathode and a hard carbon anode. *Electrochim. Acta* **56**, 7392–7396 (2011).
17. Johnson, C. S. *et al.* The significance of the Li_2MnO_3 component in 'composite' $xLi_2MnO_3 \cdot (1-x)LiMn_{0.5}Ni_{0.5}O_2$ electrodes. *Electrochem. Commun.* **6**, 1085–1091(2004).
18. Lee, D. K. *et al.* High capacity $Li[Li_{0.2}Ni_{0.2}Mn_{0.6}]O_2$ cathode materials via a carbonate co-precipitation method. *J. Power Sources* **162**, 1346–1350 (2006).
19. Zheng, J. M., Wu, X. B. & Yang, Y. A comparison of preparation method on the electrochemical performance of cathode material $Li[Li_{0.2}Mn_{0.54}Ni_{0.13}Co_{0.13}]O_2$ for lithium ion battery. *Electrochim. Acta* **56**, 3071–3078 (2011).
20. Johnson, C. S., Li, N., Lefief, C. & Thackeray, M. M. Anomalous capacity and cycling stability of $xLi_2MnO_3 \cdot (1-x)LiMO_2$ electrodes (M = Mn,Ni,Co) in lithium batteries at 50°C. *Electrochem. Commun.* **9**, 787–795 (2007).
21. Wu, Y. & Manthiram, A. High capacity, surface-modified layered $Li[Li_{(1-x)/3}Mn_{(2-x)/3}Ni_{x/3}Co_{x/3}]O_2$ cathodes with low irreversible capacity loss. *Electrochem. Solid-State Lett.* **9**, A221–A224 (2006).
22. Johnson, C. S., Li, N., Lefief, C., Vaughey, J. T. & Thackeray, M. M. Synthesis, characterization and electrochemistry of lithium battery electrodes: $xLi_2MnO_3 \cdot (1-x)LiMn_{0.333}Ni_{0.333}Co_{0.333}O_2 (0 \le x \le 0.7)$. *Chem. Mater.* **20**, 6095–6106 (2008).
23. Kim, J. H., Yi, J. H., Ko, Y. N. & Kang, Y. C. Electrochemical properties of nano-sized $LiNi_{1/3}Co_{1/3}Mn_{1/3}O_2$ powders in the range from 56 to 101 nm prepared by flame spray pyrolysis. *Mater. Chem. Phys.* **134**, 254–259 (2012).
24. Gong, Z. L., Liu, H. S., Guo, X. J., Zhang, Z. R. & Yang, Y. Effects of preparation methods of $LiNi_{0.8}Co_{0.2}O_2$ cathode materials on their morphology and electrochemical performance. *J. Power Sources* **136**, 139–144 (2004).
25. Yu, L., Qiu, W., Lian, F., Huang, J. & Kang, X. Understanding the phenomenon of increasing capacity of layered $0.65Li[Li_{1/3}Mn_{2/3}]O_2 \cdot 0.35Li(Ni_{1/3}Co_{1/3}Mn_{1/3})O_2$. *J. Alloys Compd.* **471**, 317–321 (2009).
26. Li, D. C., Muta, T., Hang, L. Q., Yoshio, M. & Noguchi, H. Effect of synthesis method on the electrochemical performance of $LiNi_{1/3}Mn_{1/3}Co_{1/3}O_2$. *J. Power Sources* **132**, 150–155 (2004).
27. Son, M. Y., Hong, Y. J., Choi, S. H. & Kang, Y. C. Effects of ratios of Li_2MnO_3 and $Li(Ni_{1/3}Mn_{1/3}Co_{1/3})O_2$ phases on the properties of composite cathode powders in spray pyrolysis. *Electrochim. Acta* **103**, 110–118 (2013).
28. Son, M. Y., Choi, S. H., Yun, J. Y., Lee, H. M. & Kang, Y. C. Electrochemical properties of nanosized Li_2MnO_3-$Li(Ni_{1/3}Co_{1/3}Mn_{1/3})O_2$ composite cathode powders prepared by spray pyrolysis. *Int. J. Electrochem. Sci.* **8**, 703–719 (2013).
29. Shin, Y. J. *et al.* Investigation on the microscopic features of layered oxide $Li[Ni_{1/3}Co_{1/3}Mn_{1/3}]O_2$ and their influences on the cathode properties. *Solid State Ionics* **177**, 515–521 (2006).
30. Yabuuchi, N., Makimura, Y. & Ohzuku, T. Solid-state chemistry and electrochemistry of $LiCo_{1/3}Ni_{1/3}Mn_{1/3}O_2$ for advanced lithium-ion batteries III. Rechargeable capacity and cycleability. *J. Electrochem. Soc.* **154**, A314–A321 (2007).
31. Lim, J. H., Bang, H., Lee, K. S., Amine, K. & Sun, Y. K. Electrochemical characterization of Li_2MnO_3-$Li[Ni_{1/3}Co_{1/3}Mn_{1/3}]O_2$-$LiNiO_2$ cathode synthesized via co-precipitation for lithium secondary batteries. *J. Power Sources* **189**, 571–575 (2009).
32. Kim, J. M. & Chung, H. T. Role of transition metals in layered $Li[Ni,Co,Mn]O_2$ under electrochemical operation. *Electrochim. Acta* **49**, 3573–3580 (2004).
33. Yu, X. *et al.* Understanding the rate capability of high-energy-density Li-rich layered layered $Li_{1.2}Ni_{0.15}Co_{0.1}Mn_{0.55}O_2$ cathode materials. *Adv. Energy Mater.* **4**, 1300950 (2014).

Acknowledgments

This work was supported by a National Research Foundation of Korea (NRF) grant funded by the Korea government (MEST) (No. 2012R1A2A2A02046367). This work was supported by the Energy Efficiency & Resources Core Technology Program of the Korea Institute of Energy Technology Evaluation and Planning (KETEP), granted financial resource from the Ministry of Trade, Industry & Energy, Republic of Korea (201320200000420).

Author contributions

M.Y.S. performed the experiments and analyzed the data. J.K.L. and Y.C.K. devised the concept, designed the experiment, analyzed the data, and wrote the manuscript.

Additional information

Supplementary information accompanies this paper at http://www.nature.com/scientificreports

Competing financial interests: The authors declare no competing financial interests.

How to cite this article: Son, M.Y., Lee, J.-K. & Kang, Y.C. Fabrication and electrochemical performance of $0.6Li_2MnO_3$-$0.4Li(Ni_{1/3}Co_{1/3}Mn_{1/3})O_2$ microspheres by two-step spray-drying process. *Sci. Rep.* **4**, 5752; DOI:10.1038/srep05752 (2014).